Journal of Materials Science and Chemical Engineering, 2014, 2, 19-27
Published Online December 2014 in SciRes. http://www.scirp.org/journal/msce
http://dx.doi.org/10.4236/msce.2014.212004

Scientific Research

Fischer-Tropsch Synthesis over Alumina-Supported Cobalt-Based Catalysts: Effect of Support Variables

Yan Liu, Heqin Guo, Litao Jia, Zhancheng Ma, Yong Xiao, Congbiao Chen, Ming Xia, Bo Hou, Debao Li*

Institute of Coal Chemistry, Chinese Academy of Sciences, Taiyuan, China
Email: liuyan@sxicc.ac.cn, *dbli@sxicc.ac.cn

Received November 2014

Abstract

Different kinds of aluminum precursors were obtained from precipitating ammonium bicarbonate, ammonium carbonate, and saturated ammonium bicarbonate, then, boehmite (AlO(OH)), ammonium alumina carbonate hydroxide (AACH) and their mixture were obtained, and then, different kinds of alumina were obtained after calcination. Three catalysts supported on the different alumina were obtained via impregnating cobalt and ruthenium by incipient wetness. The effects of different precipitants on composition of precursors were studied by XRD, FTIR, and TGA. The property and structure of alumina were studied by XRD and BET. The supported catalysts were studied by characterizations of XRD and H_2-TPR, and the catalytic performance for Fischer-Tropsch synthesis (FTS) were evaluated at a fix-bed reactor. The relations among the composition of precursors, the property of alumina and the catalytic performance of supported catalysts were researched thoroughly.

Keywords

Cobalt-Based Catalysts, Fischer-Tropsch Synthesis, Alumina, Precipitant

1. Introduction

The Fischer-Tropsch synthesis (FTS) has received much attention as a possible route in the synthesis of clean fuel and chemicals from synthetic gas. Cobalt-based catalysts are often the preferred choice for the production of high molecular weight hydrocarbons [1]. In generally, the Co^0 is generally recognized as the active species. In order to obtain high density active Co^0 species, the cobalt is often supported on a porous inorganic carrier, such as SiO_2, Al_2O_3, and TiO_2 [2]-[4]. And the final density of Co^0 sites is determined by the cobalt loading, cobalt dispersion, cobalt reduction, and interaction of cobalt-support [5]. So the choice of support is important for the final Fischer-Tropsch catalyst.

*Corresponding author.

How to cite this paper: Liu, Y., Guo, H.Q., Jia, L.T., Ma, Z.C., Xiao, Y., Chen, C.B., Xia, M., Hou, B. and Li, D.B. (2014) Fischer-Tropsch Synthesis over Alumina-Supported Cobalt-Based Catalysts: Effect of Support Variables. *Journal of Materials Science and Chemical Engineering*, **2**, 19-27. http://dx.doi.org/10.4236/msce.2014.212004

Alumina is one of the most common commercial carriers applied in FTS for its excellent thermal stability, high mechanical resistance, large surface area and pore size [6]. However, it was widely reported that the physical-chemical properties and catalytic performance of the alumina supported cobalt catalysts was strongly influenced by the properties of alumina. For instance, Xiong *et al*. [7] reported that the γ-Al_2O_3 with large pore sizes enhance the formation of large Co_3O_4 crystallites. And Bechara *et al*. found that the porous alumina modified the catalytic properties through their effects on the reducibility of the active phase [8]. However, most of the previously described alumina only have a unimodal pore size distribution. Porous alumina with a bimodal pore size distribution are sometimes more desirable from industrial application point of view. Moreover, the theoretical calculations have shown that catalysts with a bimodal pore size distribution consisting of both large and small pores allow a faster diffusion rate and a larger supported metal area at the same time [9]. The influence of pore size distribution of alumina on the activity and selectivity of Co/Al_2O_3 FTS catalysts is still not fully understood due to the complicated reaction on the catalysts. Thus, in order to obtain the optimum performance of the alumina supported cobalt catalyst, it is necessary to systemically study the relationships among the physical-chemical properties and pore size distribution of alumina and the catalytic properties for FTS of the alumina supported catalysts.

To achieve the above goal, the alumina with different textural and surface properties have to be obtained. There are several methods to prepare alumina such as precipitation, sol-gel, hydrothermal, gas phase and combustion ways [10]-[12]. Among them, the precipitation is the most widely used and cost-effective process for preparing alumina. For this methaod, the chemical composition of precursors have dramatic effects on the properties of the resultant alumina, which was strongly affected by the precipitants.

Some other research showed that the property of obtained alumina were very different with different precipitants [12] [13]. However, the reports on the Fischer Tropsch synthesis cobalt catalysts supported on aluminum obtained by precipitating different precipitants were very few.

Based on the above analysis, three kinds of alumina were obtained by using different precipitants, the effect of precipitants on phase of precursor was studied, the relations hip between physical property of alumina and chemical were illuminated by characterizations of XRD, FTIR, TGA, and BET. The $Co\text{-}Ru/Al_2O_3$ catalysts were obtained by impregnating cobalt and ruthenium on the alumina.The catalytic performance wasevaluated on the fix-bed reactor. and characterized by XRD and H_2-TPR. It indicated that the composition of precursors, property of alumina, and catalytic performance of the catalysts were greatly affected by the precipitants. The relationships among composition of precursors, property of alumina, and catalytic performance of the catalysts and were investigated simultaneously.

2. Experimental

2.1. Catalyst Preparation

The alumina oxide were prepared by precipitation**.** The typical process was as following: A certain amount of $Al(NO_3)_3{\cdot}9H_2O$ was dissolved into deionized water to obtain 1.0 mol/L solution, marked as solution A. A certain amount of ammonium bicarbonate was dissolved into deionized water to obtain the 3.0 mol/L solution, marked as solution B_1; Excess ammonium bicarbonate was dissolved into deionized water to form saturated solution, marked as solution B_2. A certain amount of ammonium carbonate was dissolved into deionized water to form 2.0 mol/L solution, marked as solution B_3.

Solution A and B_1, B_2, B_3 were co-precipitated at a water bath of 50˚C under a stirring speed of 400 r/min, respectively. The slurry was aged for 1 h at 70˚C, when the precipitation terminated. Then, the precipitate was washed and filtrated three times by using three fold water of original solution. The filter mass was dried at 110˚C for 12 h, the obtained precursor was marked as PAB, PSAB, and PAC, The PAB, PSAB, and PAC were calcined at 400˚C for 4 h under ambient atmosphere, the abtained alumina oxide were marked as AAB, ASAB, and AAC, respectively . solution of $Al(NO_3)_3{\cdot}9H_2O$ as aluminium salt, adopt 3.0 mol/L aqueous solution of, saturated aqueous solution of ammonium bicarbonate, and 2.0 mol/L aqueous solution of ammonium carbonate as alkaline precipitants, respectively. The precipitation was conducted.

The 20% Co - 0.1% Ru/Al_2O_3 catalysts were obtained by loading $Co(NO_3)_2{\cdot}6H_2O$ and ruthenium (III) nitrosyl nitrate solution on alumina by incipient wetness. The final catalysts were named as CAB, CSAB, and CAC, respectively.

2.2. Characterization Techniques

The BET surface areas of the prepared catalysts were measured with a Micromeritics model ASAP 2020 using nitrogen at −196˚C. Prior to measurements, all catalysts were outgassed at 423 K under 1×10^{-5} Torr residual pressure. X-ray diffraction (XRD) patterns were recorded on a DX-2700 diffractometer using a Cu Ka radiation (λ = 1.5404 Å). The spectra were scanned at a rate of 8°/min in the range 2θ = 5˚ - 80˚. Scanning electronic micrograph images were obtained using a LEO 1530 VP. Hydrogen temperature-programmed reduction (H_2-TPR) was carried out with a mixture of 5% H_2/N_2 as the reductive gas. The sample (0.025 g) was reduced in a flow of H_2/N_2 at a rate of 10 K·min^{-1}. The effluent gas was detected by thermal conductivity detector after removing the product water. FTIR (KBr-IR spectroscopy) spectra were recorded in a Shimadzu FT25 spectrometer. Thermogravimetric analyses (TGA) were carried out on a TGA-92 under an air flow of 50 mL·min^{-1}. The temperature increased from 50˚C to 800˚C at a rate of 10˚C·min^{-1}.

2.3. Catalyst Tests

The as-prepared catalysts were crushed and sieved in a size of 60 - 80 mesh. Catalysts (2 ml) were evaluated in a stainless-steel fixed-bed reactor (I.D. = 10 mm). After reducing at 400˚C for 6 h and cooling to room temperature, syngas with a H_2/CO mole ratio of 2.0 was switched. Wax and liquid products were collected by hot and cold traps, respectively. The exhaust gases were analyzed using a Carbosieve-packed column with TCD and Porapack-Q column with flame ionization detector (FID). Oil and wax were analyzed on a GC-920 chromatograph equipped with a 35 m OV-101 capillary column and FID. N_2 with a volume ratio of 4% was blended in the synthetic gas as an internal standard. The results were not collected until the time on stream was 48 h and the nitrogen balance was 100% ± 5% to ensure reliability of the data.

3. Results and Discussion

3.1. Phase and Structure of Precursors

The XRD patterns of precursors precipitated by using different precipitants were shown in **Figure 1**. As shown, different diffraction patterns were obtained when using different precipitants. The typical diffraction peaks of Boehmite (AlO(OH) 2θ = 14.4˚, 28.2˚, 38.3˚, 49.2˚, 55.2˚, 64˚, 71.9˚ [11]) was obtained in PAB, the retailed reaction process can be seen in Equation (1). While, both diffraction peaks of AlO(OH) and ammonium aluminum carbonate hydroxide (AACH, 2θ = 15.2˚, 21.8˚, 26.9˚, 30.7˚, 34.9˚, 41˚, 52.8˚, 55.3˚ [14]) were observed on PSAB. The PAC showed the typical diffraction peaks of the AACH .The different diffraction peaks on the three type of the alumina can be explained by the different Equations (1)-(3) the retailed reaction process should follow Equations (1) and (2) simultaneously. AACH were obtained when using ammonia carbonate as precipitant, the retailed reaction process can be seen in Equation (3).

In order to demonstrate the composition of precursors, the precursors was characterized by TGD/TG/DTA, and the result is shown in **Figure 2**. As it can be seen, the PAB exhibit obvious weight loss in the range of 200˚C - 300˚C, which is attributed to the decomposition of AlO(OH) [15] [16]. TGD/TG/DTA curves shown in to T. The maximum rate of water removal occurred at 250˚C, which was consistent with Kong's research result [15]. PAC exhibited sharp endothermic peak at 200˚C, which is attributed to the removal of the volatile species such as carbonates, hydroxides, ammonia and water vapors [16]. PAB exhibited two weight loss peaks, the corresponding decomposition temperature were consistent with the ones of PAB and PAC, respectively, which confirmed the XRD analysis result.

The TG, DTG, and DTA curves performance agreed and reveal the same massages about the decomposition of precursors. From the DTG and DTA curves in **Figure 2**, there was no weight loss for all the three precursors, while endothermic peaks emerged in the three samples, when the decomposition temperature was over 400˚C. It indicated that the crystal phase changed when the decomposition temperature was over 400˚C, although there was no weight loss, it also indicated that 400˚C was the optimal calcination temperature for calcining precursor.

In order to illustrate the crystal structure of the precursors, the FTIR characterization was carried out and the result was shown in **Figure 3**. The PAB，PSAB and PAC exhibited broad absorption bands around 3300 - 3500 cm^{-1}, which are assigned to stretching mode of adsorbed water [17]. For PAB, the bands at 3306, 3094, and 1070 cm^{-1} were observed, which are belong to the *v*as(Al)O-H, *v*s(Al)O-H, and *δ*sAl-O-H vibrations of AlO(OH), respectively emerge in PAB [11] [12], which claim that completed crystal of AlO(OH) formed in

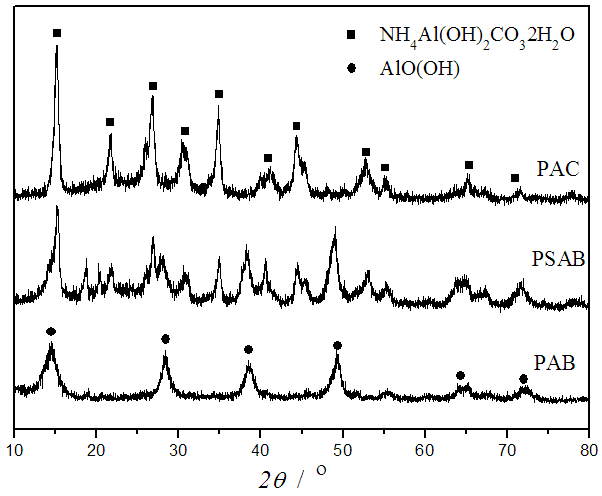

Figure 1. XRD patterns of different precursors.

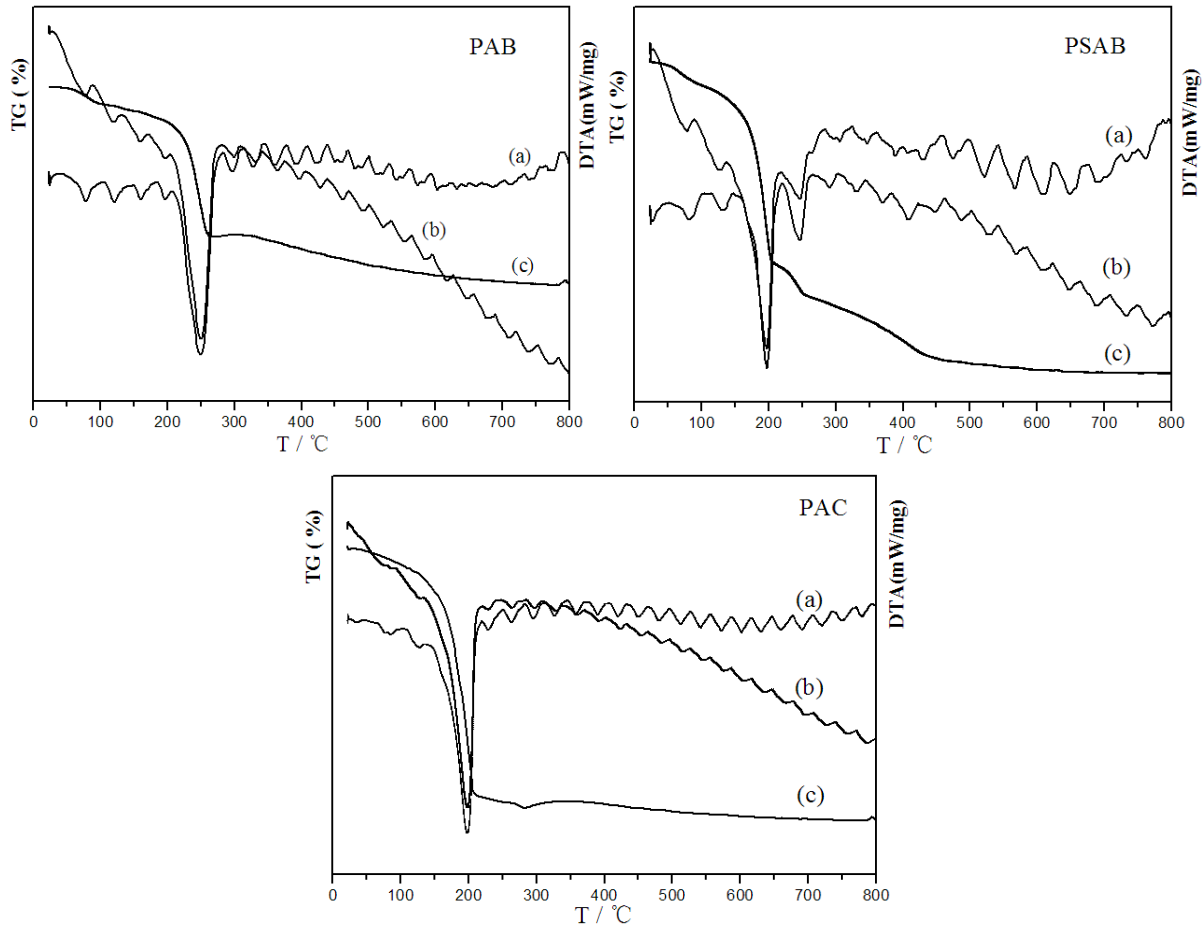

Figure 2. TGD/TG/DTA curves of different precursors.

PAB. There are obvious bond vibrations of OH-(νOH at 3443 cm^{-1}, δOH at 988 cm^{-1}) [16], NH_4^+ (νNH at 3178, 2898, and 2846 cm^{-1}, δNH at 1832 and 1724 cm^{-1}) [18], and CO_3^{2-} (ν3 at 1560, 1458 cm^{-1}, and ν1 at 1106 cm^{-1}, ν2 at 854 cm^{-1}, and ν4 at 750 cm^{-1}) [19], which indicated clearly that AACH formed in the PAC. For PSAB, δsAl-O-H vibrations of AlO(OH) at 1070 cm^{-1} occurred in its pattern, meanwhile, ν3 vibrations of

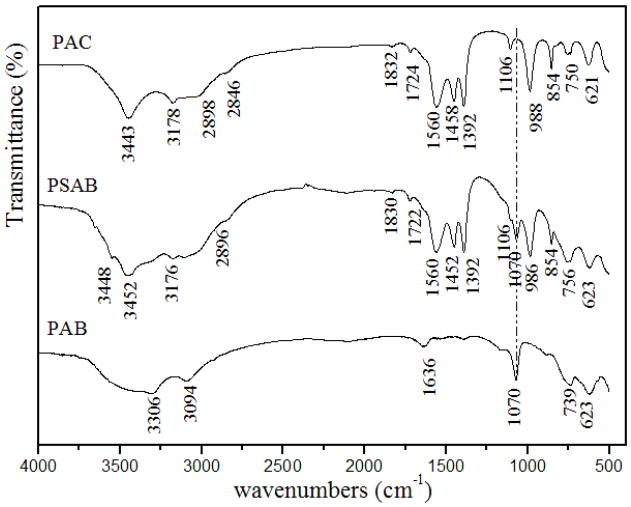

Figure 3. FTIR patterns of different precursors.

CO_3^{2-} at 1560 and 1452 cm^{-1} also occurred, indicating that both AlO(OH) and AACH existed in PSAB, which was consistent with the XRD and TGA results. The rest of bands at 621, 739 and 756 cm^{-1} are ascribed to the vibrational modes of Al-O [20].

3.2. Structure and Pore Size Distribution of Alumina

Figure 4 shows the XRD patterns of alumina obtained by calcining the precursors at 400˚C for 4 h in air. Diffraction peaks at 2θ = 37.60˚, 39.49˚, 45.80˚, 60.90˚, 67.03˚ appeared in all of three alumina [21]. However, the diffraction intensity were different from each other, the intensity of AAC was the strongest, and ASAB was the weakest. The texture property of different alumina were listed in **Table 1**. ASAB possessed the biggest surface area as 279 m^2/g, combining the weak diffraction peak in **Figure 4**, it indicated that the alumina crystals were even and dispersive, the synergy existed in the two kinds of alumina crystals was strong. Effective integration occurred in the two kinds of alumina during the process of calcining the two kinds of precursors. AAC possessed big specific surface area for releasing CO_2, NH_3, and H_2O during the calcination process, AAC also possessed big average pore diameter and pore volume for the same reason. AAB possessed smaller surface area, pore diameter, and pore volume.

The pore size distribution curves of different alumina are displayed in **Figure 6**. As shown, AAB displayed unimodal pore size distribution, the major pore size was in the range of 4 - 6 nm. AAC also displayed unimodal pore size distribution with some scare pore of 5 nm, the major pore size was 20 nm about. However, ASAB displayed bimodal pore distribution, of which the small pore was attributed to calcining AlO(OH) in PSAB, while the big one was attributed to calcining AACH in PSAB, this pore size distribution was accordance with Bai's research result [9].

3.3. Structure and Property of Supported Catalysts

The 20% Co - 0.1% Ru/Al_2O_3 catalysts were obtained by incipient wetness impregnating cobalt and ruthenium in the three alumina, the corresponding XRD patterns were shown in **Figure 6**. Diffraction peaks of Co_3O_4 at the same 2θ of 18.2˚, 31.3˚, 37˚, 45˚, 55.8˚, 59.4˚, 65.2˚ appeared in the three XRD patterns of catalysts [22]. However, the intensity of the three catalysts were not identical, the intensity of CAC was stronger than the other two, the intensity of CSAB was the weakest. The crystal size of supported Co_3O_4 particles were calculated by Scherrer equation at 2θ = 37˚. Catalyst CSAB possessed the smallest crystal size of 8.2 nm, and the crystal size of CAB and CAC were 10.5 nm and 12.9 nm, respectively. Based on the analysis of pore size distribution of different alumina, the pores of AAB were narrow, the supported Co^{2+} overflowed and accumulated on the mouth of the pores during calcination; the pores of AAC were so big that the supported Co^{2+} gathered and accumulated due to lacking of confinement in the big pores. The pore size distribution of ASAB were bimodal pore, the synergy between small pores and big pores avoided the disadvantages of unimodal pore.

Table 1. The texture property of different alumina.

Sample	BET surface area (m^2/g)	Average pore diameter (nm)	Pore volume (m^3/g)
AAB	218	5.2	0.53
ASAB	279	8.6	0.88
AAC	256	14.7	0.91

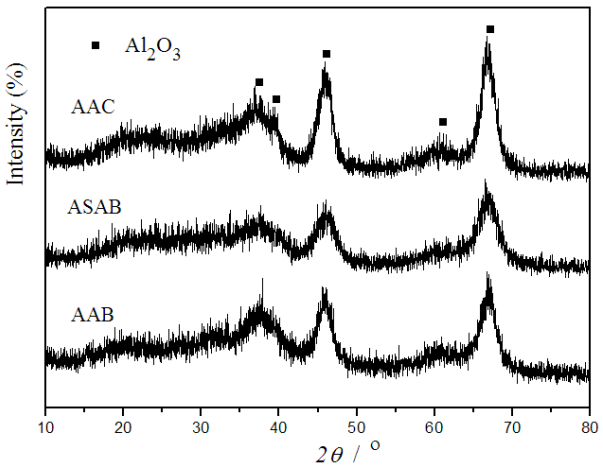

Figure 4. XRD patterns of different precursors.

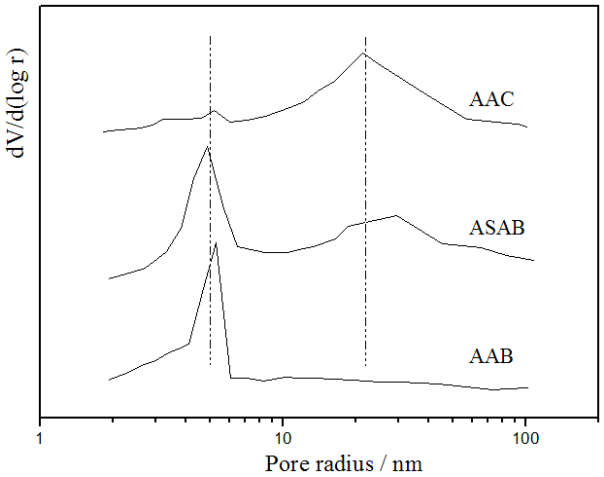

Figure 5. Pore size distribution of different alumina.

The TPR curves of the three Co-Ru/Al_2O_3 catalysts were shown in **Figure 7**. The reduction peaks for Co_3O_4 can be assigned to two-step reduction in this work, the reduction peaks emerged in two major temperature ranges: 180˚C - 250˚C and 260˚C - 460˚C. According to the reported literature [23], the first peak is assigned as the reduction process of Co_3O_4 to CoO, the second peak is assigned as the reduction process of CoO to Co. As shown in **Figure 7**, both of the first reduction peak and the second one of CSAB were the lowest temperature among the three catalysts. This is because the cobalt particle size was small and was easy to reduce. In another aspect, cobalt particles of CSAB were more dispersive than the others for its proper pore structure and big specific surface area. The second-step reduction temperature of CAB was much lower than that of CAC for its smaller cobalt crystal. There existed a weak reduction peak at 550˚C around, which is associated with surface cobalt aluminate difficult to be reduced [24] [25]. It is assumed to be highly dispersed and interact strongly with alumina.

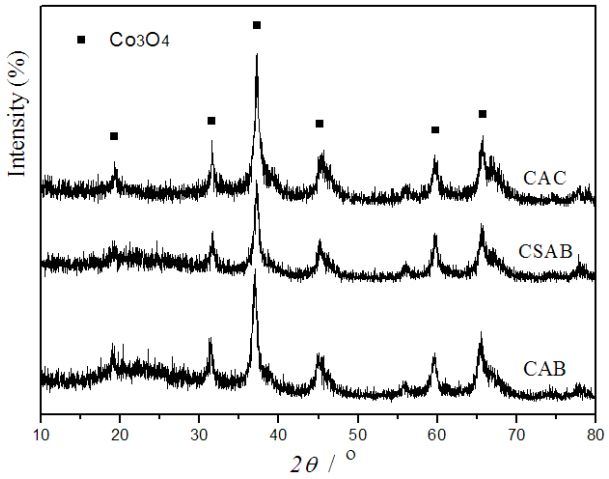

Figure 6. XRD patterns of different catalysts.

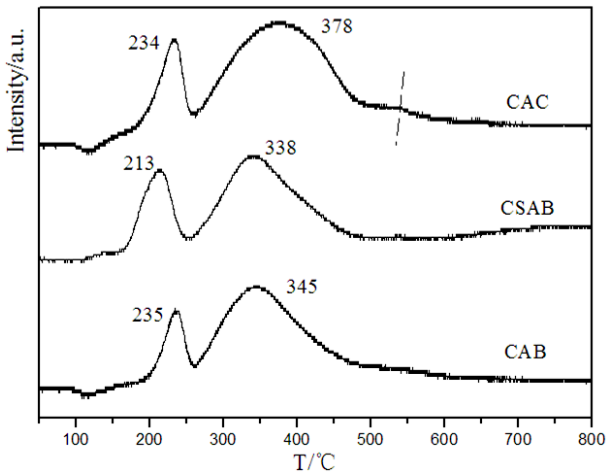

Figure 7. H_2-TPR curves of different catalysts.

3.4. Catalytic Performance of Catalysts

The FTS catalytic performance of different catalysts were summarized in **Table 2**. Catalyst CSAB reached a much higher CO conversion than the other two catalysts, under the same reaction temperature its CO conversion was 51.4%. The order of CO conversion was CSAB > CAB > CAC. This was because CSAB possessed proper cobalt particle size, big specific surface area, and lower reduction temperature, which benefited to improve the catalytic performance for FTS.

The order of methane selectivity was CSAB < CAB < CAC, this order was just right opposite to the order of CO conversion. As shown in **Figure 5**, the pores of AAB were narrow, the supported catalyst possessed much narrower pores, which restricted the mass transfer, thus, the CO conversion was low. The cobalt crystals were aggregated for lacking of restriction in the large pores, the exposure active sites were scarce, thus, the CO conversion was also low. The pore structure of ASAB was bimodal pore distribution, the active sites dispersed on both small and big pores, thus, little molecule product produced in narrow pore entered big pores and grew up further, the big pores and the small pores were in an effective synergy.

4. Conclusion

Pure AlO(OH) can be prepared by using ammonium bicarbonate as precipitant, and pure AACH can be prepared by using ammonium carbonate as precipitant, while a mixture of AlO(OH) and AACH can be obtained by using saturated ammonium bicarbonate as precipitant. The alumina obtained by calcining mixture of AlO(OH) and

Table 2. Catalytic performance of Co-Ru/Al_2O_3 catalysts for Fischer-Tropsch synthesis.

Catalysts[a]	CO Conversion/%	Hydrocarbon distribution/wt%			CO_2 selectivity /wt%
		CH_4	C_2 - C_4	C_5^+	
CAB	45.5	6.6	6.9	86.5	0.7
CSAB	51.4	6.0	6.3	87.7	0.8
CAC	38.9	8.1	8.7	83.2	0.6

[a]Reaction conditions: 200˚C, 2 MPa, GHSV=1000 h^{-1}, CO/H_2 = 2.

AACH possessed bimodal pore size distribution, the biggest specific surface area of 279 m^2/g, the smallest cobalt particle size of 8.2 nm, and the lowest reduction temperature of 213˚C, which benefited to acquire the highest CO conversion of 51.4% and the lowest CH_4 selectivity of 6.0% for Fischer-Tropsch synthesis at the same conditions. The performance was much more excellent than that supported on alumina via calcining pure AlO(OH) or AACH. In conclusion, alumina obtained from calcining a mixture of AlO(OH) and AACH obtained by co-precipitation would be expected to be a prospective alumina carrier for the FTS cobalt-based catalysts.

Acknowledgements

The authors would like to acknowledge the financial support from the National Natural Science Foundation of China (Grant No. 21203232).

References

[1] Borg, Ø., Ery, S., Blekkan, E.A., Storsæter, S., Wigum, H., Rytter, E. and Holmen, A. (2007) Fischer-Tropsch Synthesis over γ-Alumina-Supported Cobalt Catalysts: Effect of Support Variables. *Journal of Catalysis*, **248**, 89-100. http://dx.doi.org/10.1016/j.jcat.2007.03.008

[2] Bartholomew, C.H. and Reuel, R.C. (1985) Cobalt-Support Interactions: Their Effects on Adsorption and CO Hydrogenation Activity and Selectivity Properties. *Industrial & Engineering Chemistry Product Research and Development*, **24**, 56-61. http://dx.doi.org/10.1021/i300017a011

[3] Pansanga, K., Panpranot, J., Mekasuwandumrong, O., Satayaprasert, C., Goodwin, J.G. and Praserthdam, P. (2008) Effect of Mixed γ- and χ-Crystalline Phases in Nanocrystalline Al_2O_3 on the Dispersion of Cobalt on Al_2O_3. *Catalysis Communications*, **9**, 207-212. http://dx.doi.org/10.1016/j.catcom.2007.05.042

[4] Storsæter, S., Borg, Ø., Blekkan, E.A., Tøtdal, B. and Holmen, A. (2005) Fischer-Tropsch Synthesis over Re-Promoted Co Supported on Al_2O_3, SiO_2 and TiO_2: Effect of Water. *Catalysis Today*, **100**, 343-347. http://dx.doi.org/10.1016/j.cattod.2004.09.068

[5] Storsæter, Ø., Tøtdal, B., Walmsley, J.C., Tanem, B.S. and Holmen, A. (2005) Characterization of Alumina-, Silica-, and Titania-Supported Cobalt Fischer-Tropsch Catalysts. *Journal of Catalysis*, **236**, 139-152. http://dx.doi.org/10.1016/j.jcat.2005.09.021

[6] Cheng, N.Y., Ma, C., Han, Q. and Li, X.N. (2012) Synthesis and Application of γ-Al_2O_3 Supported CoRu-Based Fischer-Tropsch Catalyst. *Chemical Engineering Journal*, **191**, 534-540. http://dx.doi.org/10.1016/j.cej.2012.03.024

[7] Xiong, H.F., Zhang, Y.H., Wang, S.G. and Li, J.L. (2005) Fischer-Tropsch Synthesis: The Effect of Al_2O_3 Porosity on the Performance of Co/Al_2O_3 Catalyst. *Catalysis Communications*, **6**, 512-516. http://dx.doi.org/10.1016/j.catcom.2005.04.018

[8] Bechara, R., Balloy, D. and Vanhove, D. (2001) Catalytic Properties of Co/Al_2O_3 System for Hydrocarbon Synthesis. *Applied Catalysis A*: *General*, **207**, 343-353. http://dx.doi.org/10.1016/S0926-860X(00)00672-4

[9] Bai, P., Wu, P.P., Yan, Z.F. and Zhao, X.S. (2009) A Reverse Cation-Anion Double Hydrolysis Approach to the Synthesis of Mesoporous γ-Al_2O_3 with a Bimodal Pore Size Distribution. *Microporous and Mesoporous Materials*, **118**, 288-295. http://dx.doi.org/10.1016/j.micromeso.2008.08.047

[10] Urretavizcaya, G., Cavalieri, A.L., Porto López, J.M., Sobrados, I. and Sanz, J. (1998) Thermal Evolution of Alumina Prepared by the Sol-Gel Technique. *Journal of Materials Synthesis and Processing*, **6**, 1-7. http://dx.doi.org/10.1023/A:1022674107059

[11] Tang, Z., Liang, J.L., Li, X.H., Li, J.F., Guo, H.L., Liu, Y.Q. and Liu, C.G. (2013) Synthesis of Flower-Like Boehmite (γ-AlOOH) via a One-Step Ionic Liquid-Assisted Hydrothermal Route. *Journal of Solid State Chemistry*, **202**, 305-314.

http://dx.doi.org/10.1016/j.jssc.2013.03.049

[12] Ji, G.J., Li, M.M., Li, G.H., Gao, G.M., Zou, H.F., Gan, S.C. and Xu, X.H. (2012) Hydrothermal Synthesis of Hierarchical Microflower-Like γ-AlOOH and γ-Al_2O_3 Superstructures from Oil Shale Ash. *Powder Technology*, **215-216**, 54-58. http://dx.doi.org/10.1016/j.powtec.2011.09.005

[13] Li, J.-G., Ikegami, T., Lee, J.-H., Mori, T. and Yajima, Y. (2000) Co-Precipitation Synthesis and Sintering of Yttrium Aluminum Garnet (YAG) Powders: The Effect of Precipitant. *Journal of the European Ceramic Society*, **20**, 2395-2405. http://dx.doi.org/10.1016/S0955-2219(00)00116-3

[14] Stoica, G. and Pérez-Ramírez, J. (2007) Reforming Dawsonite by Memory Effect of AACH-Derived Aluminas. *Chemistry of Materials*, **19**, 4783-4790. http://dx.doi.org/10.1021/cm071351g

[15] Kong, J., Chao, B.X., Wang, T. and Yan, Y.L. (2012) Preparation of Ultrafine Spherical AlOOH and Al_2O_3 Powders by Aqueous Precipitation Method with Mixed Surfactants. *Powder Technology*, **229**, 7-16. http://dx.doi.org/10.1016/j.powtec.2012.05.024

[16] Varma, H.K., Mani, T.V., Damodaran, A.D., Gopa, K. and Warrier, K. (1994) Characteristics of Alumina Powders Prepared by Spray-Drying of Boehmite Sol. *Journal of the American Ceramic Society*, **77**, 1597-1600. http://dx.doi.org/10.1111/j.1151-2916.1994.tb09762.x

[17] Kim, D.S. and Lee, G.D. (2014) Study on γ-Alumina Precursors Prepared Using Different Ammonium Salt Precipitants. *Journal of Industrial and Engineering Chemistry*, **20**, 1269-1275. http://dx.doi.org/10.1016/j.jiec.2013.07.003

[18] Abdullah, M., Mehmood, M. and Ahmad, J. (2012) Single Step Hydrothermal Synthesis of 3D Urchin Like Structures of AACH and Aluminum Oxide with Thin Nano-Spikes. *Ceramics International*, **38**, 3741-3745. http://dx.doi.org/10.1016/j.ceramint.2012.01.019

[19] Du, X.L., Wang, Y.Q., Su, X.H. and Li, J.G. (2009) Influences of pH Value on the Microstructure and Phase Transformation of Aluminum Hydroxide. *Powder Technology*, **192**, 40-46. http://dx.doi.org/10.1016/j.powtec.2008.11.008

[20] Bradley, S.M., Kydd, R.A., Russell and Howe, F. (1993) The Structure of Al Gels Formed through the Base Hydrolysis of Al^{3+} Aqueous Solutions. *Journal of Colloid and Interface Science*, **159**, 405-412. http://dx.doi.org/10.1006/jcis.1993.1340

[21] Kul'ko, E.V., Ivanova, A.S., Litvak, G.S., Kryukova, G.N. and Tsybulya, S.V. (2004) Preparation and Microstructural and Textural Characterization of Single-Phase Aluminum Oxides. *Kinetics and Catalysis*, **45**, 714-721. http://dx.doi.org/10.1023/B:KICA.0000044984.09163.80

[22] Wey, R.S., Teoh, Y., Mädler, L., Grunwaldt, J.-D., Amal, R. and Pratsinis, S.E. (2008) Ru-Doped Cobalt-Zirconia Nanocomposites by Flame Synthesis: Physicochemical and Catalytic Properties. *Chemistry of Materials*, **20**, 4069-4079. http://dx.doi.org/10.1021/cm8002657

[23] Kim, Y.H. and Park, E.D. (2010) The Effect of the Crystalline Phase of Alumina on the Selective CO Oxidation in a Hydrogen-Rich Stream over Ru/Al_2O_3. *Applied Catalysis B*: *Environmental*, **96**, 41-50. http://dx.doi.org/10.1016/j.apcatb.2010.02.001

[24] Hemmati, M.R., Kazemeini, M., Khorasheh, F. and Zarkesh, J. (2013) Investigating the Effect of Calcination Repetitions on the Lifetime of Co/γ-Al_2O_3 Catalysts in Fischer-Tropsch Synthesis Utilising the Precursor's Solution Affinities. *Journal of the Taiwan Institute of Chemical Engineers*, **44**, 205-213. http://dx.doi.org/10.1016/j.jtice.2012.11.003

[25] Barroso, M.N., Gomez, M.F., Arru'a, L.A. and Abello, M.C. (2006) Reactivity of Aluminum Spinels in the Ethanol Steam Reforming Reaction. *Catalysis Letters*, **109**, 13-19. http://dx.doi.org/10.1007/s10562-006-0051-9